ISSN: 0067-2904

Influence of Cylindrical Electrode Configuration on Plasma Parameters in a Sputtering System

Alaa Khamees Bard*, Qusay Adnan Abbas
Department of Physics, College of Science, University of Baghdad, Baghdad, Iraq

Received: 2/11/2021 Accepted: 5/3/2022 Published: 30/8/2022

Abstract

In the present work, the effect of the cylindrical configurations of the sputtering device electrodes on the plasma parameters (Debye length, electron temperature, electron density, plasma frequency) is studied. Also, the effect of the argon gas pressure on the discharge properties is examined with gas pressures of (0.08, 0.2, 0.4 and 0.6) Torr. The properties of the plasma are diagnosed by optical emission spectrometry. The spectroscopic method is adopted for examining the atomic spectra of argon emission. The electron temperature is determined by the Boltzmann method. While, the Stark-widening method was employed for calculating the electron number density. The voltage against current curves of the cylindrical sprayer discharges shows the voltage to be nearly constant with slight increase in current. An increase in pressure causes the cathode cascades to compress and the negative glow to become thinner and more luminous. Plasma properties such as electron temperature and Debye length decrease with increasing pressure, while electron number density and plasma frequency increase.

Keywords: cylindrical sputtering system, Boltzmann plot method, electron number density, Electron temperature.

تأثير ترتيب الأقطاب على خصائص البلازما في نظام الترذيذ الاسطواني

الاء خميس برد*, قصي عدنان عباس
[1]قسم الفيزياء, كلية العلوم, جامعة بغداد، بغداد، العراق

الخلاصة

في العمل الحالي تمت دراسة تأثير التكوينات الأسطوانية لاقطاب جهاز الترذيذ على معاملات البلازما (طول ديباي ، درجة حرارة الإلكترون ، كثافة الإلكترون ، تردد البلازما). كما تم فحص تأثير ضغط الغاز على خواص التفريغ يكون لضغط غاز بقيم (0.08 ، 0.2 ، 0.4 و 0.6) تور. تم تشخيص خصائص البلازما بواسطة مطياف الانبعاث البصري. اعتمدت الطريقة الطيفية لفحص الأطياف الذرية لانبعاث الأرجون ، ومخطط بولتزمان لتحديد درجة حرارة الإلكترون ، وطريقة ستارك التوسيع لحساب كثافة عدد الإلكترون. تبين من منحنى الجهد والتيار لتفريغ الترذيذ الأسطواني ان الجهد ثابتٌ تقريبًا مع زيادات طفيفة في التيار. تؤدي الزيادة في الضغط إلى انضغاط منطقة الكاثود ويصبح التوهج السالب أرق وأكثر إضاءة. تنخفض خصائص البلازما مثل درجة حرارة الإلكترون وطول ديباي مع زيادة الضغط ، بينما تزداد كثافة عدد الإلكترون وتردد البلازما.

*Email: alaa.bard1104@Sc.uobaghdad.edu.iq

1.Introduction

The sputtering process is a crucial phenomenon that occurs in glow discharge tubes when the voltage delivered to the cathode is high enough. When the plasma ions and the fast neutrals collide with the cathode target, secondary electrons and atoms are liberated from the cathode. Physical vapor deposition (PVD) is when the species sputtered off a cathode target are employed as film-forming material. Spraying becomes easier When the cathode target is subjected to gas discharge, either a D.C. or an A.C. discharges [1,2]. Magnetron sputtering discharge (MSD) [3], ion beam sputter deposition, on the other hand, is a well-known PVD process [4]. Evaporation is another PVD technology, ion plating, pulsed laser deposition, and cathodic arc deposition. The low deposition rate of MSD, DC diode sputter high working gas pressure and high discharge voltage [5]. MSD is typically used in a glow discharge mode [6]. Many early demonstrations and analyses of cylindrical magnetron formation [7] and the first magnetron sputtering [8,9,10] were fabricated using cylindrical magnetron formations with axial magnetic fields. These discharges are of two types, the first is using the outer cylinder as the target of the cathode, and it is called post cylindrical configuration [11] and the second, the cylindrical hollow arrangement (also known as an inverted magnetron), in which the cathode target is located on the outside cylinder [5].

2.Experimental Setup

The cylindrical sputtering system was designed and built. The chamber of this system consists of two coaxial stainless steel cylinders. The cylindrical magnetron consists of two configurations; the first, the post-discharge configuration, consists of a cylindrical cathode mounted coaxially inside the anode. This arrangement can cover a large area on a small substrate. The second configuration, the inverted-discharge configuration, consists of a cylindrical anode coaxially installed inside the cathode. Figure 1a shows a diagram of the two configurations of the electrodes, Figure 1b is a photograph of the two electrodes in a cylindrical sputtering device. The inner and outer cylinders have a diameter of 3 cm and 25 cm, respectively, and a length of 22 cm. The vacuum gas utilized in this apparatus is argon gas, which has a purity of 99.998% and may be used at different pressures.

Two different types of glow discharge appear in a cylindrical system. The first is a positive space charge dominated mode (PSC mode), whereas the second is a negative space charge dominated mode (NSC mode). When a constant voltage of around 3 kV was applied between two axial electrodes, the normal mode of glow discharge was produced. The glow-discharge cleaning procedure was used to clean the device's chamber.

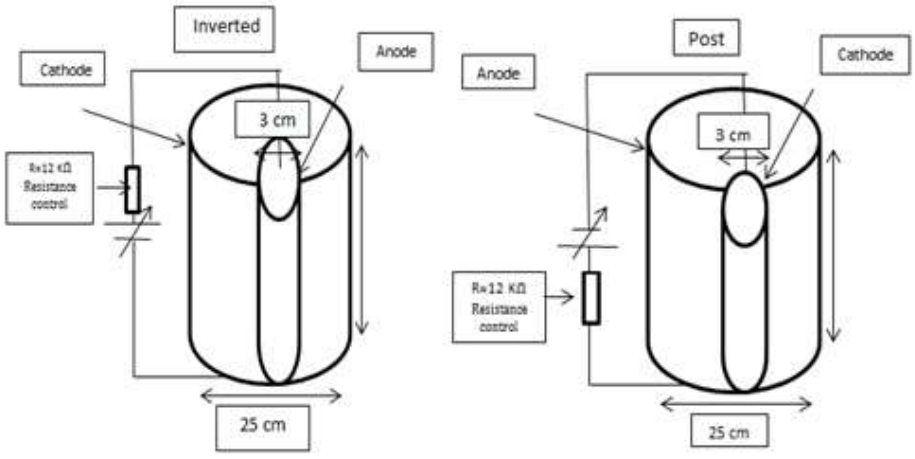

Figure 1- a) Schematic diagram of the two electrode configuration for a cylindrical sputtering device .

Figure 1- b) Photograph of two electrodes in a cylindrical sputtering device .

3. Theoretical Description of Plasma Parameters

When a plasma is subjected to a local potential, the oppositely charged particles organize to confine the electric field (**E**). The potential resulting from the thermal oscillation of highly mobile electrons is shielded to a distance called the Debye length (λ_D). The Debye length in the plasma can be obtained by equality the kinetic energy of the thermal electrons with resulting electrostatic potential as follows [12]:

$$\lambda_D = \sqrt{\frac{\varepsilon_0 k_B T_e}{e^2 n_e}} \tag{1}$$

Where: k_B is Boltzmann's constant, ε_0 is the permittivity of free space, e is the electronic charge, T_e is the electron temperature and n_e the electron number density. The electron waves play a fundamental role in many plasma interactions with electromagnetic waves at the plasma frequency ω_{pe} defined as [13]:

$$\omega_p = \sqrt{\frac{n_e e^2}{m_e \epsilon_0}} \tag{2}$$

where m_e is the electron mass.

the electron temperature (T_e) is the most important factor used to describe the state of plasma. T_e can be calculated according to the method of the Boltzmann diagram as follows [14,15]:

$$\ln\left(\frac{I_z \lambda_{Ki,z}}{g_{K,Z} A_{Ki,Z}}\right) = -\frac{1}{k_B T_e} E_{k,z} + \ln\left(\frac{hcL_{nZ}}{4\pi P_Z}\right) \tag{3}$$

Table 1 explains the equation parameters.

Table 1- Physical meaning of the parameters of Equation (3)

Z	represent the species-related ionization state
C	the light's speed
k_B	Boltzmann constant
L	the plasma's characteristic length
H	Planck's constant
$E_{k,Z}$, $g_{k,Z}$	represent the energy and degeneracy of the upper energy level k, respectively
PZ	reflects the species partition function in ionization stage Z.
IZ	The optically measured integrated intensity of a species in ionization stage Z

If the left-hand side of Equation (3) is plotted for several transformations against the higher-level energy of the species in the Z ionization phase, the result is a straight line, the slope of which represents T_e in eV. Also, the Stark expansion relationship is used to calculate the electron number density assuming that the Stark expansion is the dominant effect [16]:

$$n_e(cm^{-3}) = \left[\frac{\Delta\lambda}{2\omega_s(\lambda_D T_e)}\right] N_r \quad (4)$$

Where: ω_s represents the Stark expansion parameter, $\Delta\lambda$ represents the full width at half maximum of the line, N_r represents the reference electron number density, which is equal to 10^{16} cm^{-3} for neutral atoms and 10^{17} cm^{-3} for singly charged ions.

4. Results and Discussion

4.1 Glow discharge structure

The basic principle of this device is the glowing discharge between the two electrodes. In this device, the argon plasma discharge column is produced when a constant D.C voltage of about 3kV is applied between the two coaxial electrodes in the two electrode configurations. As a result of this applied voltage, an electric field is generated and causes an electrical breakdown in the argon gas. The different argon gas pressure applied was 0.08, 0.2, 0.4 and 0.6 Torr. Photographs of the glow discharge at these pressures for the post-configuration are presented in Figure 2. It can be seen that as the pressure increases, the cathode regions are compressed (the falling cathode), the negative glow turns into a thin layer of strong luster, and the positive column, the incident anode grow. This is because the average free path of the electrons is inversely proportional to the pressure of the gas; hence the distance an electron must travel before producing enough ionization to maintain the glow is inversely proportional to the pressure. That is, when the pressure rises, the thickness of the cathode dark region shrinks (i.e. the falling cathode is compressed). Therefore, the negative glow area will turn into a small layer of intense luster, while the positive column area will grow, and the anode will fall off. This result is in agreement with that of Abbas [17].

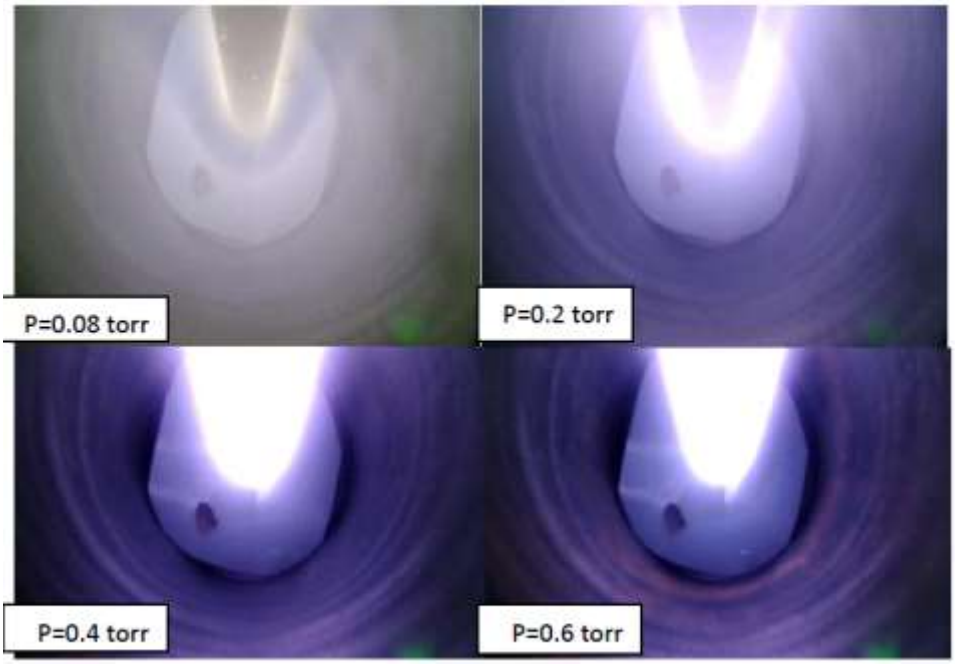

Figure 2- photographs of the glow discharge in the post cylindrical sputtering device at different pressures.

Figure 3 shows the glow discharge regions in the inverted cylindrical sputtering configuration. Upon closer examination, it can be seen that as the pressure increases, the anode regions are compressed (anode fall), the positive glow turns into a thin layer of dense luster, while the negative column increases and the cathode fall decrease.

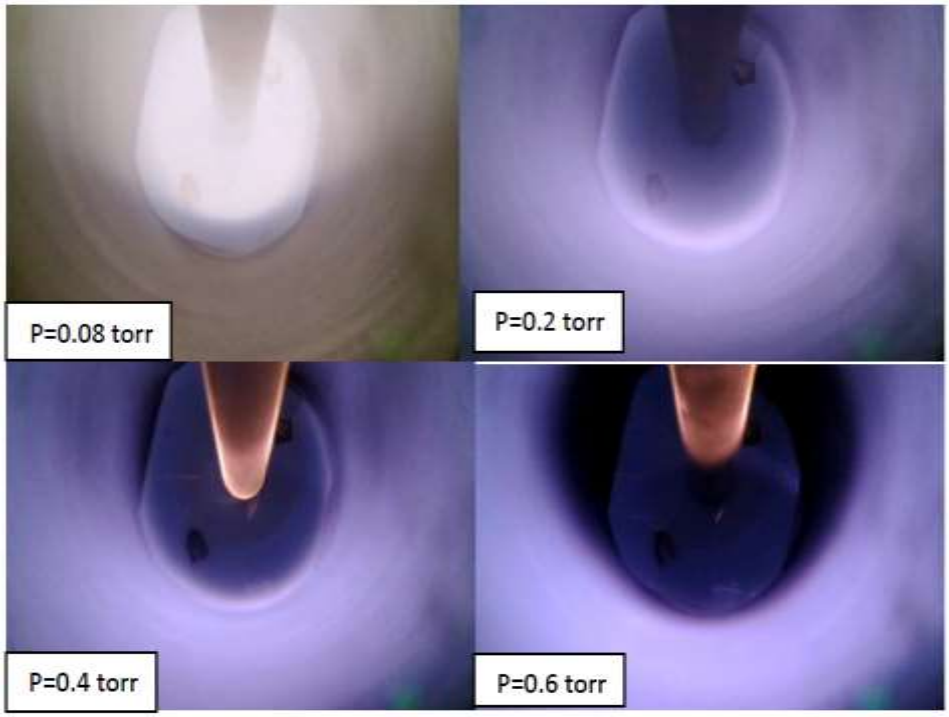

Figure 3-Photographs of the glow discharge in the inverted cylindrical sputtering device at different pressures.

4.2 Discharge processes

Figure 4 shows the variation of the discharge voltage with the product (pd) of the argon pressure (p) and the negative electrode separation (d) of the cylindrical sprayer. One can notice that the discharge voltage increases when pd is increased. This result means that the higher ionization efficiency of the cylindrical spray discharge occurs for low values of pd. Because for high values of pd, the pendulum movement of electrons is attenuated. It is also noticed, from this figure, that the discharge voltage in the case of post arrangement is less than in the inverted case. This shows that the Paschen curve does not change by changing the shape of the electrodes, as it gives results similar to those of the planar electrodes [18].

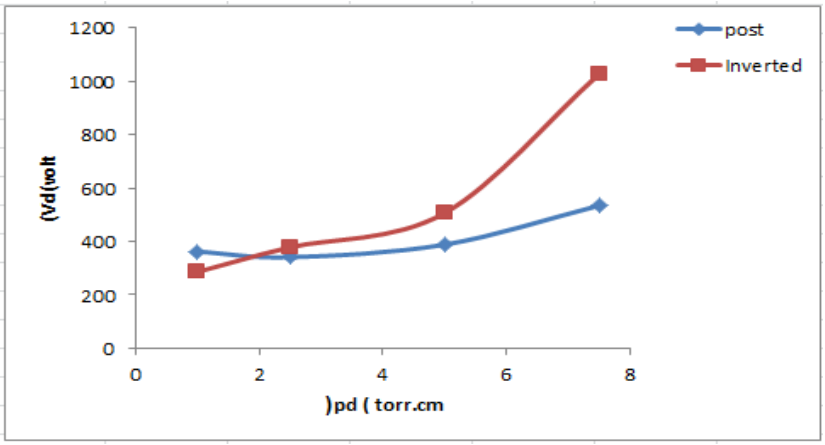

Figure 4-Variation of discharge voltage with product p.d for the two cylindrical electrode configurations

Figure 5 shows the discharge voltage as a function of the discharge current in the cylindrical sputtering for different gas pressures. The fact that the usual glow discharge is produced with constant voltage and increasing current is obvious. In this condition, the discharge is analogous to a regular glow discharge between cylindrical electrodes. The discharge current increases as the gas pressure is increased from 0.08 Torr to 0.6 Torr, while the discharge operating voltage remains nearly constant.

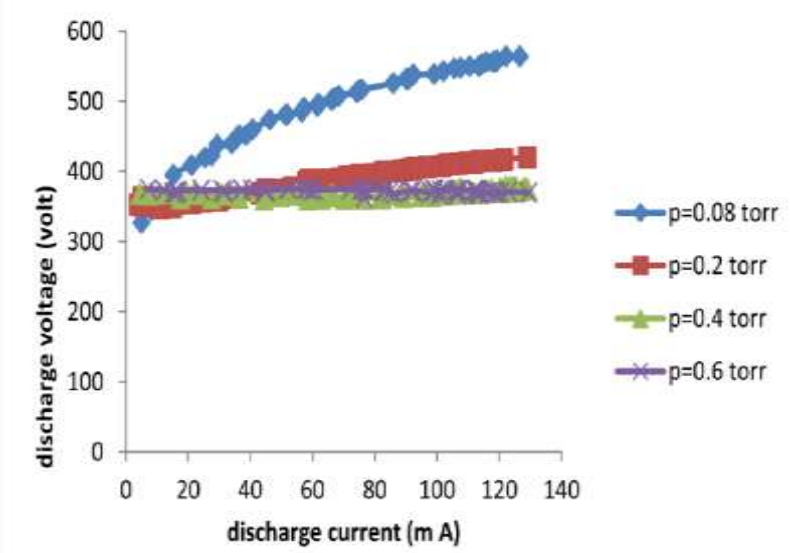

Figure 5-Variation of target voltage as a mapping of discharge current in post configuration electrodes for various gas pressures.

Figure 6 shows the discharge voltage as a function of the discharge current for the inverted cylindrical electrodes for different gas pressures. From the figure, it can be seen that the behaviour is similar to the discharging behavior in the case of a post-cylindrical configuration, but in pressure 0.08 Torr and 0.2 Torr, the behaviour is abnormal.

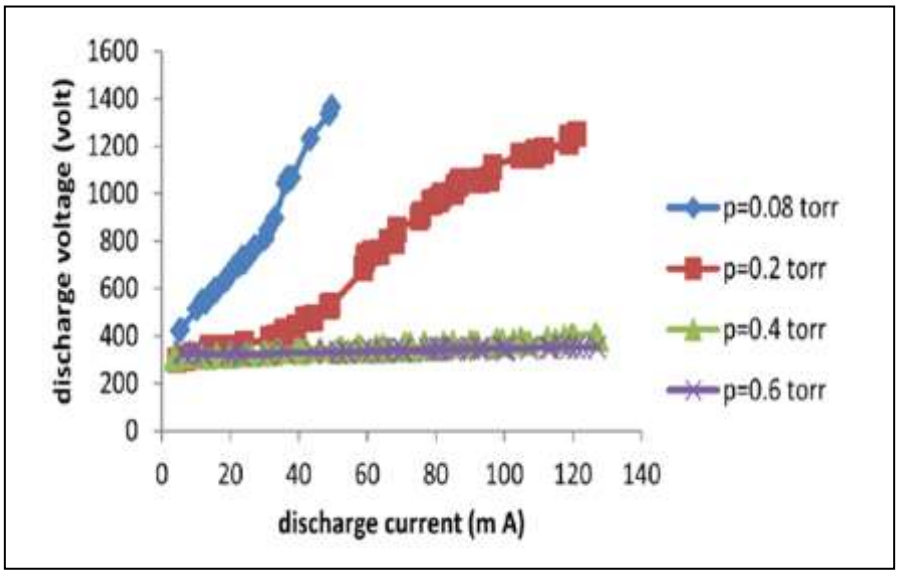

Figure 6-The variation of target voltage as a function of discharge current for different gas pressures in the inverted configuration electrodes.

4.3 Plasma emission spectra

Figure 7 depicts the emission spectra in the 320–740 nm wavelength region of the post-discharge configuration at different argon gas pressures. The spectra show seven neutral argon (Ar I) emission peaks at wavelengths 546.71600, 557.25410, 617.94190, 659.61130, 677.99260, 703.02510, 735.08140 nm and four argon (Ar II) ionic emission lines with wavelength 361.18130, 405.76750, 427.75280, 470.23160 nm. According to the spectra, as the gas pressure increases, the strength of all peaks in the ArI and ArII lines increases. In ArI the light emission intensity is much lower than that in ArII. All peaks intensity increases with increasing the gas pressure from 0.08 to 0.6Torr. The probability of collision between electrons and gas atoms increases due to the increase in the electron number density, which increases with the increase in gas pressure, allowing electrons to have sufficient excitation energy.

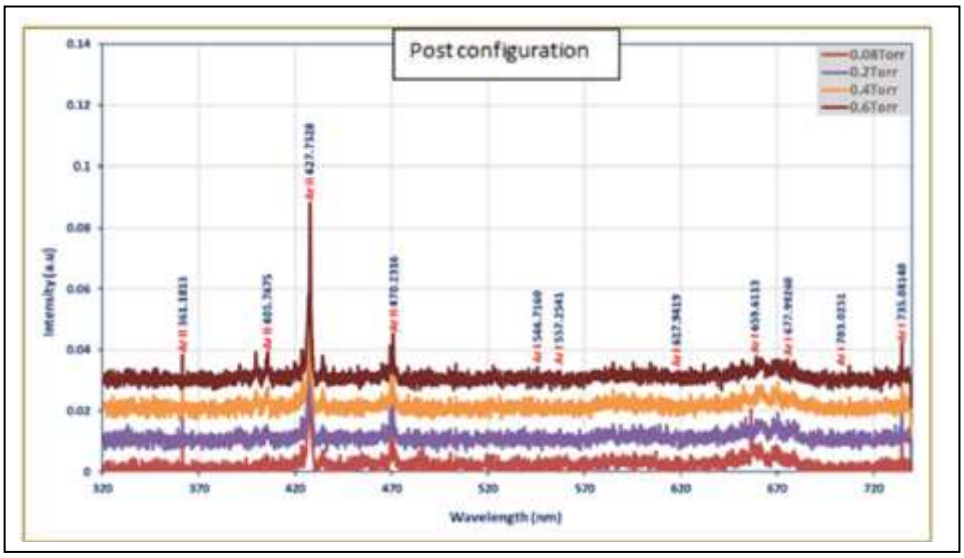

Figure 7-Optical emission spectra of Ar plasma for post-discharge configuration at different gas pressures.

Figure 8 depicts the emission spectra in the 320–740 nm wavelength region of the inverted-discharge configuration at different argon gas pressures. The spectra are identical to those of post-discharge configuration.

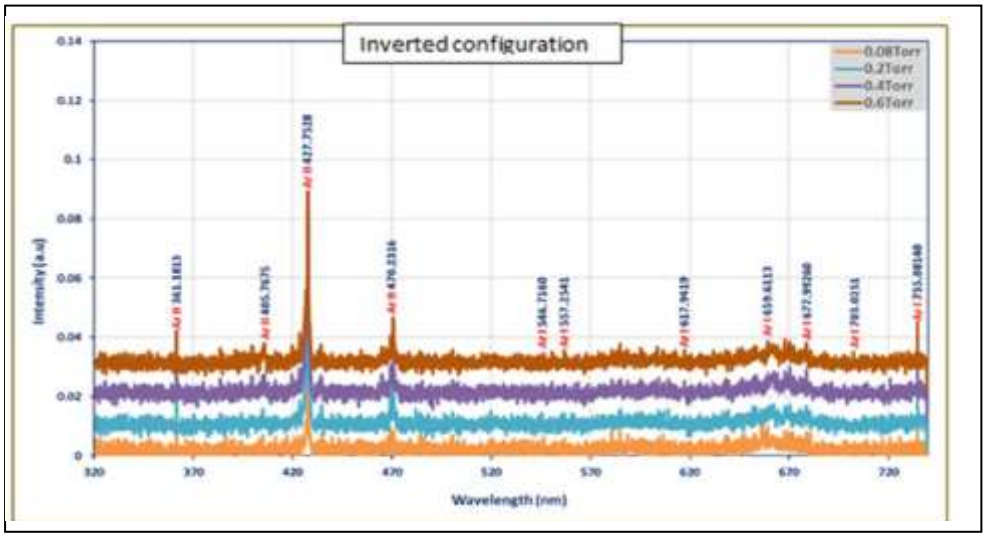

Figure 8-Optical emission spectra of Ar plasma for the inverted-discharge configuration at different gas pressures.

4.4 Plasma parameters in the two different configurations

Electron temperature is the most important parameter of plasma which is used to describe the state of the plasma .

A variety of plasma excitation and ionization processes are controlled by the electron temperature (T_e). Assume the plasma is at local thermodynamic equilibrium, the number of excited atoms follows the Boltzmann distribution to compute T_e. Using the data in Table 2, the method of Boltzmann plot was used to calculate the value of T_e (equation (3).

Table 2-Ar I standard lines are used to calculate electron temperature, and their characteristics. [19]

λ(nm)	$A_{ji}g_i$	E_i(eV)	E_j(eV)
546.71600	38×10^6	13.09487256	15.3620414
557.25410	4.6×10^6	13.09487256	15.31916801
617.94190	0.2×10^6	13.30222747	15.30807770
659.61130	0.11×10^6	13.07571571	14.95485204
677.99260	0.363×10^6	13.47988682	15.30807770
703.02510	13.4×10^6	13.07571571	14.83881100
735.08140	1.2×10^6	13.32785705	15.0140655

Figure 9 demonstrates the Boltzmann plots for the post-discharge configuration utilizing selected atomic argon lines (ArI) in situations under investigation at different gas pressures.

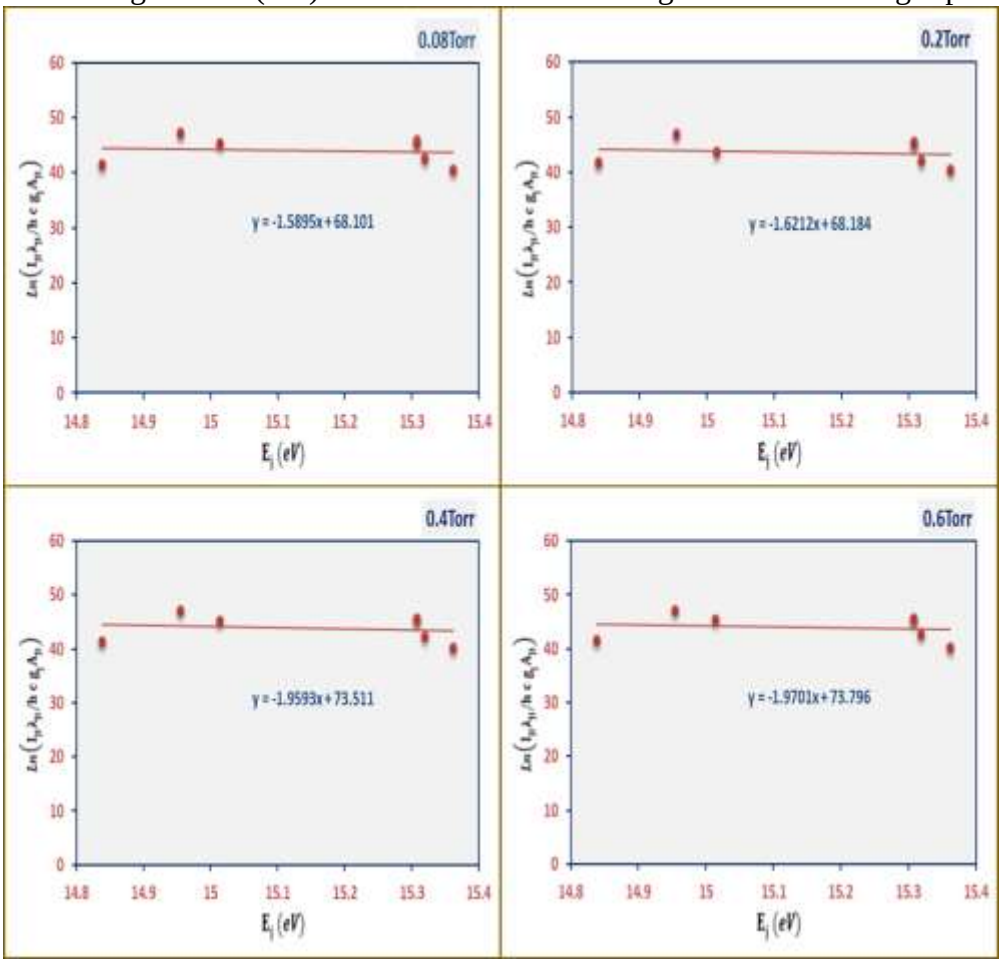

Figure 9-Boltzmann plots for post-discharge configuration using selected atomic argon lines (ArI) at different gas pressures.

Figure 10 shows the Boltzmann plots for the inverted-discharge configuration using the selected atomic argon lines (ArI) under study at different gas pressures.

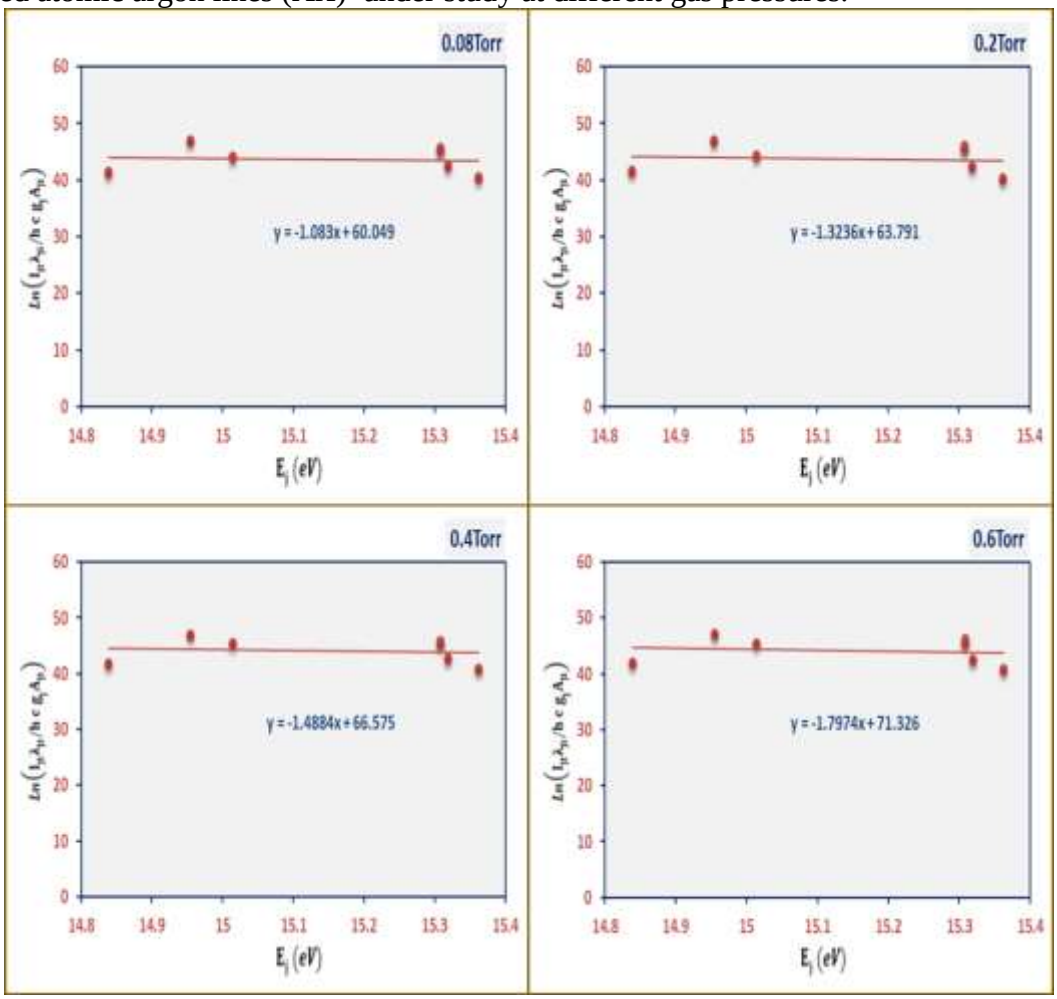

Figure 10-Boltzmann plots for the inverted-discharge configuration using the selected atomic argon lines (ArI) under study at different gas pressures.

The use of spectroscopic atomic lines emitted from the plasma is one of the most reliable techniques for determining the electron number density (n_e). Equation (4) is used to calculate electron number density, which is called the Stark broadening effect. FWHM (The full width at half maximum) values were used to calculate the electron number density using the Stark effect depending on the standard values of broadening for this line ($Nr=10^{16}cm^{-3}$) [19]. The effect of argon gas pressure on electron number density and electron temperature is shown in Figure 11 in the post-discharge configuration. The curve shows an increase in n_e with rising pressure from 0.08 to 0.6 Torr, while the temperature of the electron decreased as the gas pressure increased. This trend can be explained by the fact that increased gas pressure causes more inelastic collisions between electrons and Ar atoms, resulting in a higher electron number density.

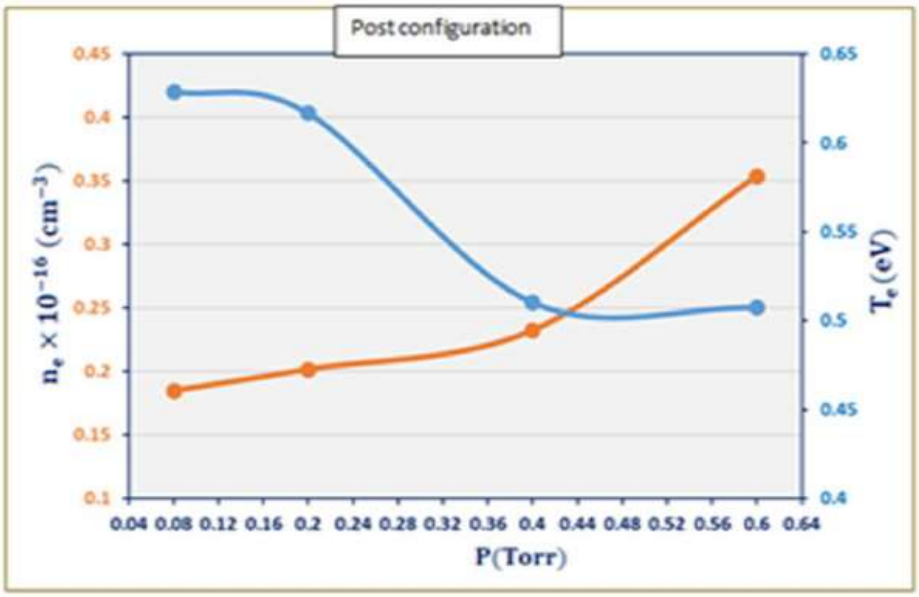

Figure 11- Variation of n_e and T_e in post-discharge configuration as a function of gas pressure.

Figure 12 depicts the effect of argon gas pressure on the behaviour of electron temperature and electron number density in the inverted-discharge configuration. The curve shows an increase in n_e with rising pressure from 0.08 to 0.6 Torr, in contrast the temperature of the electron decreased.

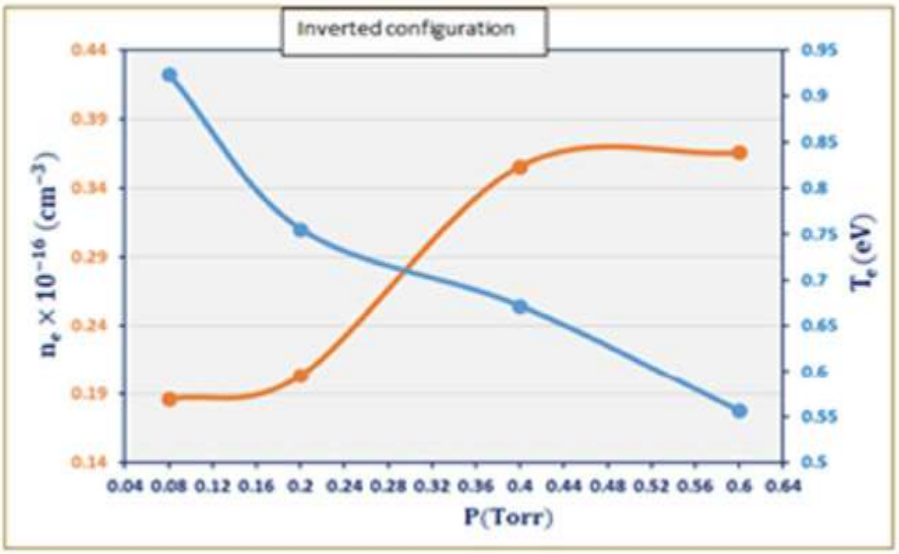

Figure 12- Variation of n_e and T_e in the inverted-discharge configuration as a function of gas pressure.

The Debye length ($\boldsymbol{\lambda}_D$) was calculated using Equation (1) and Table 3. The results for the post-discharge configuration show that the Debye length decreases with increasing the gas pressure from 0.08 to 0.6 Torr. The decrease in Debye length is related to the increase in inelastic collisions, which restrict the plasma in a small area, resulting in an increase in plasma density due to the plasma confinement. On the other hand, the plasma frequency ω_{pe} was calculated using Equation (2), and the result showed that the plasma frequency increases with increasing the argon gas pressure [20] .

Table 3- Variation of ω_{pe} and $\boldsymbol{\lambda_D}$ against the gas pressure in post-discharge configuration.

$\mathbf{P}$ $(\mathbf{Torr})$	$\mathbf{T_e}$ $(\mathbf{eV})$	$\mathbf{n_e \times 10^{16}}$ $(\mathbf{cm^{-3}})$	$\boldsymbol{\omega_{pe} \times 10^{11}}$ $(\mathbf{rad/sec})$	$\boldsymbol{\lambda_D \times 10^{-6}}$ $(\mathbf{cm})$
0.08	**0.9234**	**0.1862**	**24.3919**	**16.5439**
0.2	**0.7555**	**0.2036**	**25.5041**	**14.3119**
0.4	**0.6719**	**0.3558**	**33.7139**	**10.2102**
0.6	**0.5564**	**0.3657**	**34.1818**	**9.1641**

In the case of the inverted- discharge configuration, Table 4 shows the change in both Debye length and plasma frequency as pressure increases. It is clear from the table that the Debye length and plasma frequency have the same behavior as those of the post-discharge configuration. However, the values in the case of post-discharge configuration are higher than those of the inverted-discharge configuration .

Table 4- the variation of ω_{pe} and $\boldsymbol{\lambda_D}$ against the gas pressure in inverted configuration electrodes

P (Torr)	**T_e (ev)**	$\boldsymbol{n_e \times 10^{16}}$ $(\mathbf{cm^{-3}})$	$\boldsymbol{\omega_{pe} \times 10^{11}}$ $(\mathbf{rad/sec})$	$\boldsymbol{\lambda_D \times 10^{-6}}$ $(\mathbf{cm})$
0.08	**0.6291**	**0.1849**	**24.3039**	**13.7049**
0.2	**0.6168**	**0.2018**	**25.3895**	**12.9899**
0.4	**0.5104**	**0.2324**	**27.2457**	**11.0116**
0.6	**0.5076**	**0.3537**	**33.6136**	**8.9009**

5.Conclusions

This paper presents the effect of the gas pressure and the electrodes configuration on the plasma parameter in a cylindrical sputtering system. The discharge properties were investigated based on the spectroscopic measurements of the plasma generated inside the chamber. The results showed that the discharge properties behave in the same way for both electrode configurations. The results also showed that the discharge properties change by changing the gas pressure. The behavior of the discharge properties strongly depends on the discharge processes that occur inside the cavity. The results showed that the post rank is the best as it has the highest ionization efficiency.

6.References

[1] E. Kay, "Impact evaporation (sputtering) and thin film growth in a glow discharge," *In:Marton, L.L. (Ed.), Advances of Electronics and Electron Physics*, Academic Press, New York, vol. 17, pp. 245–322, 1962.

[2] Y. K. Jabur, M. G. Hammed, and M. K. Khalaf, "DC Glow Discharge Plasma Characteristics in Ar/O2 Gas Mixture," *Iraqi Journal of Science*, vol. 62, no. 2, PP. 475-482, 2021.

[3] R.K. Waits, "Planar magnetron sputtering," *Journal of Vacuum Science and Technology*, vol. 15, no. 2, pp. 179–187, 1978.

[4] C. Bundesmann, H. Neumann, "The systematics of ion beam sputtering for deposition of thin films with tailored properties," *Journal of Applied Physics*, vol. 124, no. 23, p. 231102, 2018.

[5] J. T. Gudmundsson,"Physics and technology of magnetron sputtering discharges," *Plasma Sources Sci. Technol*., vol. 29, no. 11, p.113001, 2020.

[6] J. T. Gudmundsson and A. Hecimovic, "Foundations of DC plasma sources," *Plasma Sources Sci. Technol*. Vol. 26 , no.12, 2017.

[7] J. A. Thornton, "Magnetron sputtering: basic physics and application to cylindrical magnetrons," *Journal of Vacuum Science and Technology*, vol. 15, p. 171, 1978.

[8] J. A. Thornton,"The influence of bias sputter parameters on thick copper coatings deposited using a hollow cathode," *Thin Solid Films*, vol. 40, pp. 335–344, 1977.

[9] K. Wasa and S. Hayakawa, "Reactively sputtered titanium resistors, capacitors and rectifiers for microcircuits," *Microelectron. Reliab.*, vol. 6, no. 3, pp. 213–214, 1967.
[10] Q. A. Abbas, R. R. Abdula and B. T. Chied ,"The axial profile of plasma characteristics of cylindrical magnetron sputtering device," *Iraqi Journal of Science*, vol. 8, no.11, PP. 41 – 47 , 2010.
[11] K. Wasa and S. Hayakawa, "Low Pressure Sputtering System of the Magnetron Type," *Review of Scientific Instruments*, vol. 40, no. 5, p. 693, 1969.
[12] K.H. Spatschek, "Introduction to Theoretical Plasma Physics", lecture series, 2008.
[13] C. Fallon, "Optical Diagnostics of Colliding Laser Produced Plasmas: Towards Next Generation Plasma Light Sources," Ph.D. thesis, Dublin City University, 2013.
[14] N. Idris, T.N. Usmawanda, K. Lahna, M. Ramli ,"Temperature estimation using Boltzmann plot method of many calcium emission lines in laser plasma produced on river clamshell sample," *Journal of Physics: Conference Series*, vol. 1120, p. 012098, 2018.
[15] N. Ohno, M.A. Razzak , H. Ukai , S. Takamura , Y. Uesugi ,"Validity of electron temperature measurement by using boltzmann plot method in radio frequency inductive discharge in the atmospheric pressure range," *Plasma Fusion Res*., vol. 1, p. 028, 2006.
[16] A.M. El Sherbini, A.A.S. Al Aamer, A.T. Hassan, T.M. El Sherbini, "Measurements of plasma electron temperature utilizing magnesium lines appeared in laser produced aluminum plasma in air," *Optics and Photonics Journal*, vol. 2, no. 4, p. 278, 2012.
[17] Q. A. Abbas, "Plasma Characteristics of a DC Closed Field Magnetron Sputtering Device," Ph.D. Thesis, University of Baghdad, Iraq, 2009.
[18] Q. A. Abbas, A. F. Ahmed, F. A.-H. Mutlak," Electromagnetic hollow cathode discharge spectroscopy Properties of plasma," *Optik - International Journal of Optical and Electronic Optics*, 242 (2021) 167260, 2021.
[19] https://www.nist.gov/pml/atomic-spectra-database .
[20] N. Konjevic, A. Lesage, J. Fuhr, and W. Wiese, "Experimental Stark widths and shifts for spectral lines of neutral and ionized atoms," *J. Phys. Chem. Ref. Data*, vol. 19, no. 6, PP. 1307–1385, 1990. (A Critical Review of Selected Data for the Period 1989 Through 2000)